

Article

Mechanically-Induced Catalyzation of MgH₂ Powders with Zr₂Ni-Ball Milling Media

M. Sherif El-Eskandarany ^{*}, Fahad Al-Ajmi and Mohammad Banyan 

Nanotechnology and Advanced Materials Program, Energy and Building Research, Center, Kuwait Institute for Scientific Research, Safat 13109, Kuwait; ftajmi@kisar.edu.kw (F.A.-A.); mbanyan@kisar.edu.kw (M.B.)

* Correspondence: msherif@kisar.edu.kw

Received: 15 April 2019; Accepted: 22 April 2019; Published: 24 April 2019



Abstract: Magnesium hydride (MgH₂) holds immense promises as a cost-effective hydrogen storage material that shows excellent storage capacity suitable for fuel cell applications. Due to its slow hydrogen charging/discharging kinetics and high apparent activation energy of decomposition, MgH₂ is usually doped with one or more catalytic agents to improve its storage capacity. So often, milling the metal hydride with proper amounts of catalyst leads to heterogeneous distribution of the catalytic agent(s) in MgH₂ matrix. The present work proposes a cost-effective process for doping Mg powders with Zr₂Ni particles upon ball milling the powders with Zr₂Ni-balls milling media under pressurized hydrogen. Fine Zr₂Ni particles were gradually eroded from the balls and homogeneously embedded into the milled powders upon increasing the ball milling time. As a result, these fine hard intermetallic particles acted as micro-milling media and leading to the reduction the Mg/MgH₂ powders. Meanwhile, Zr₂Ni eroded particles possessed excellent heterogeneous catalytic effect for improving the hydrogenation/dehydrogenation kinetics of MgH₂. This is implied by the short time required to absorb (425 s)/desorb (700 s) 6.2 wt% H₂ at 200 °C and 225 °C, respectively. The as-milled MgH₂ with Zr₂Ni balls possessed excellent cyclability, indexed by achieving continuous 646 cycles in 985.5 h (~1.5 cycle per hour) without serious degradation.

Keywords: reactive ball milling; ball milling media; arc melting; intermetallic compound; micro-milling media; in-situ catalyzation; hydrogen storage nanocomposites; thermal stability; de/rehydrogenation kinetic; cycle-life-time

1. Introduction

Hydrogen storage nanocrystalline and nanocomposite materials are current area of tremendous research interest in chemistry, energy, materials science and the environment. Reference to its natural abundance, low cost, high gravimetric (7.60 wt%) and volumetric (110 g/L) hydrogen storage capacities, magnesium (Mg) metal has been receiving great attention for four decades as a promising hydrogen storage material. Reactive ball milling (RBM), which was investigated in the beginning of the 1990s [1,2] is a cost effective process, employed for conducting gas–solid reactions at ambient temperature, starting from pure metal and desired gas. Since then, RBM has been intensively used to produce large amounts of high quality MgH₂ nanocrystalline powders, starting from Mg metal and hydrogen gas [3–5].

In contrast to the many attractive properties found in MgH₂ material, it is seldomly used in desired fuel cell application without intensive treatment [6–10]. This is attributed to high activation energy, high decomposition temperature and slow absorption/desorption kinetics [11–14]. Severe plastic deformation (SPD) technique [15], including high energy ball milling [16], cold rolling (CRing) [17,18], high pressure torsion (HPT) [19] and equal channel angular pressing (ECAP) [20] were employed to improve the hydrogen storage properties of MgH₂. Apart from the mechanical treatment approach, catalyzation MgH₂ powders with proper volume fractions of catalytic agents [21], including pure

metals [22], intermetallic compounds [23–26], metal-oxides [27,28], metal/metal oxide composites [5,29], -carbides [30,31], metallic glassy alloys [32–34] and chlorides [35] have shown outstanding effects on enhancing the hydrogen storage properties of MgH_2 and infer its apparent activation energy of decomposition [36]. More recently, self-assembled MgH_2 and metal borohydride nanoparticles on graphene technique has shown great enhancement of the behavior of the metal hydride phase [37–39].

1.1. Mechanically-Induced Catalyzation (MIC) of Mg/MgH_2 Powders

MIC catalyzation refers to doping Mg/MgH_2 powders with desired catalytic agent(s), using high-energy ball milling operated under inert or hydrogen gas for at least 10 h. Like any other chemical processing, the activity of the catalyst is expected to be linearly increased with increasing its amount added to MgH_2 . Efficiency of the catalytic agent active sites is not only depending on the amount used, but it is mainly affected by the degree of their dispersion homogeneity in the matrix (Mg/MgH_2). In many cases, pure metal and metal powder alloys added to MgH_2 and then milling are affected by the cold welding taken place during the milling process. Accordingly, they tend to be agglomerated to form large powder particles and are heterogeneously distributed in a few zones in the Mg/MgH_2 matrix. Such heterogeneous distribution of catalytic agents leads to produce either rich or poor active site Mg/MgH_2 powders.

1.2. Ball-Milling Media as a Source of Catalysts

In 2016, El-Eskandarany and his team replaced tool steel balls with Ni-balls milling media for RBM process of Mg powders under pressurized hydrogen gas [40]. They pointed out that Mg/MgH_2 powders were homogeneously catalyzed with eroded Ni fine particles upon ball–powder–ball collisions [41]. This approach inhibited the agglomeration of metallic catalytic agent and ensured the formation of very uniform nanocomposite powders.

In the present work, we attempted to investigate the possibility of doping Mg powders with tetragonal- Zr_2Ni , using Zr_2Ni balls-milling media as a source of solid catalysts. The catalytic effect on the hydrogen storage properties, indexed by hydrogenation/dehydrogenation kinetics measured at different RBM times and temperatures were studied. Moreover, the effect of RBM time on decomposition temperature and apparent activation energy of MgH_2 were investigated. In addition, the cyclability of MgH_2 milled with Zr_2Ni balls is reported.

2. Results and Discussion

2.1. Hydrogenation Kinetics of MgH_2 during the RBM Process

Effect of Milling Media (MM)

For the purpose of the present work, an arc melting technique was used to fabricate Zr_2Ni master alloy buttons, started from pure Zr and Ni bulk metals. The materials were placed in a Cu-hearth cooled by water, where the melting process (Figure 1a,b) was conducted for six times to ensure homogeneity of the product. The fabricated Zr_2Ni master alloys had nearly spherical-like shape ~10 mm in diameter (Figure 1c). These spherical-balls were used as milling media (MM) for conducting RBM of Mg powders under pressurized (50 bar) H_2 (Figure 1d). Details of these experiments are described in the Materials and Methods section.

In all experiments, high-pressure milling vial equipped with a gas-temperature-monitoring (GTM) system was used to monitor the progress of the mechanically induced gas–solid-reaction taking place between Mg and H_2 during different stages of RBM time. This was indicated by the pressure change (desorption) and time required for absorption at a specific RBM time. In addition, the GTM system allowed us to realize the effect of MM (tool steel and Zr_2Ni balls) on the mechanically-induced hydrogenation process.

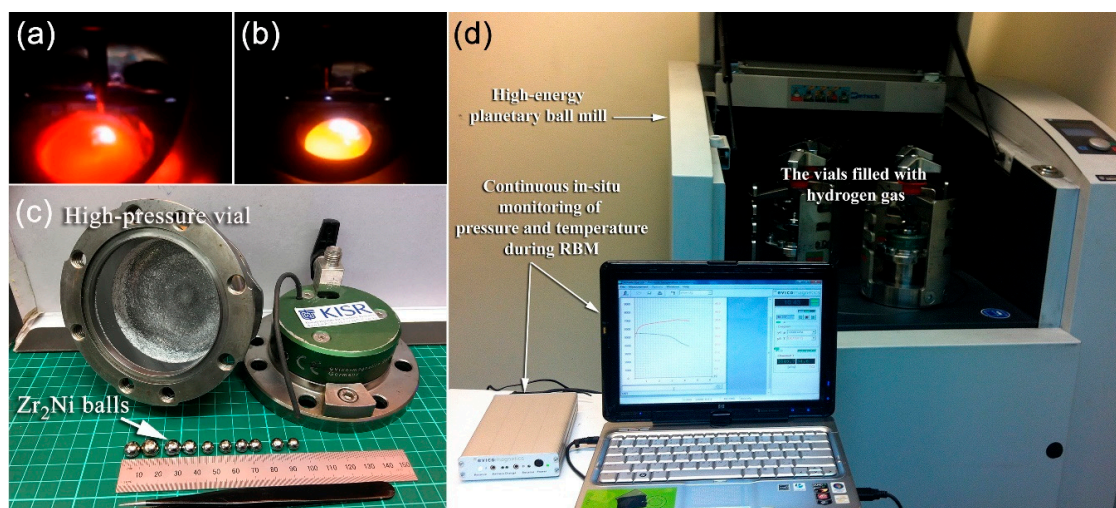


Figure 1. Bulk Zr and Ni (Zr_2Ni) during (a) melting and (b) solidification in the He-arc melter. The obtained Zr_2Ni buttons were almost perfect spheres with nearly 10 mm in diameter (c). Zr_2Ni balls-milling media (50 pieces) were sealed in a 200 mL high-pressure vial made of tool steel (c) together with different 5 g of Mg powders. The system was pressurized with 50 bar of hydrogen gas and then mounted on a planetary high-energy ball mill operated at room temperature for 25, 37.5 and 50 h of reactive ball milling (RBM) time (d). The experiments were repeated 2–4 times to ensure reproducibility of each milling run, using milling media (MM)-to-powder (P) weight ratio as 40:1.

Figure 2a elucidates the effect of RBM time on the vial's pressure during RBM of Mg under 5000 kPa of H_2 , using MM-to-P as 40:1. At the first stage of RBM, the vial's pressure slightly dropped from 5000 kPa to ~4900 kPa after 3.2 h (Figure 2a). At this early stage of RBM, the powders were subjected to severe lattice imperfections due to the effect of ball–powder–ball collisions (Figure 2b). Meanwhile, the hydrogen pressures inside the vials employed tool steel and Zr_2Ni as MM were 4799 and 4391 kPa, respectively (Figure 2a).

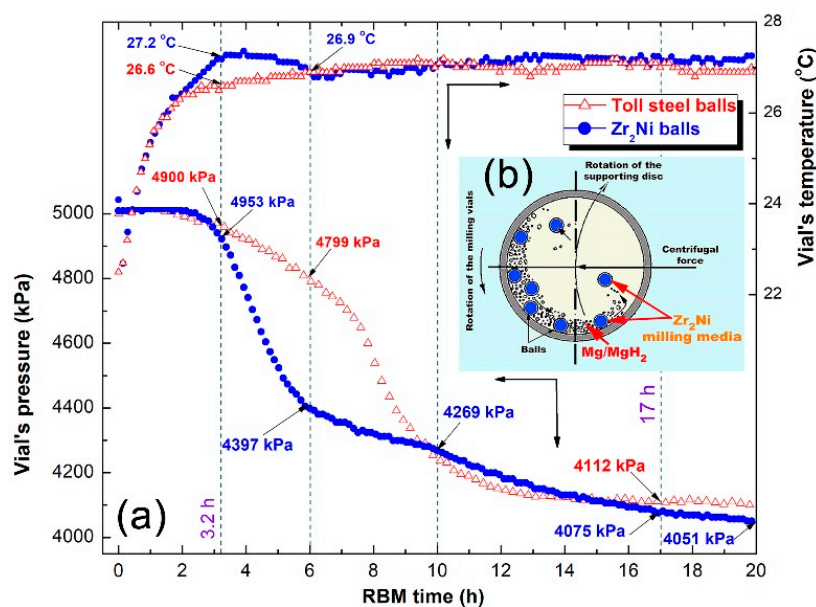


Figure 2. (a) The effect of milling media materials (tool steel and Zr_2Ni) on the kinetics of hydrogenation of Mg powders induced by the RBM process. Schematic presentation shows ball–powder–ball collisions and their movements inside the vial during the RBM process conducted under 5000 kPa hydrogen pressure, using a planetary high-energy ball mill, is presented in (b). The MM-to-P was 60:1.

After 6 h, this drastic decrease in pressure upon using Zr_2Ni MM is believed to be related to three factors; (i) a greater number of active Mg surfaces were created and guttered (absorbed) much more hydrogen when compared with the powders milled with tool steel MM, (ii) a certain amount of hard Zr_2Ni fine powders came from corroded Zr_2Ni balls and introduced to Mg powders may have played a vital catalytic role for splitting hydrogen molecules into atoms and (iii) the presence of such refractory Zr_2Ni hard powders in the Mg/MgH₂ powder matrix played the role of micro-media, in which they led to accelerate reduction of powder sizes into the sub-micro level.

In the intermediate stage of RBM, the sample milled with Zr_2Ni MM slightly guttered much more hydrogen upon milling for 10 h, as indicated by the drop in vial pressure (4269 kPa), as shown in Figure 2a. After this stage, the vial's pressure of Mg milled with tool steel balls reached almost the same value (4269 kPa), which suggested that both samples milled with different MM have absorbed almost the same amount of hydrogen (Figure 2a). During the last stage of RBM (14 to 20 h) the slight decrease in the vial's pressure was monitored (~4000 kPa) for both samples, which suggested completion of the gas–solid-reaction process, as displayed in Figure 2a.

2.2. Crystal Structure

X-ray diffraction (XRD) was employed to study the effect of RBM time on structural changes of Mg powders obtained after 6 h (early stage), 12.5 h and 25 h (intermediate stage) and 50 h (final stage) of RBM. The XRD pattern of the sample obtained after 6 h of milling (Figure 3a) revealed Bragg peaks corresponding to pure hcp-Mg with no evidence of MgH₂ present, as shown in Figure 3a. The XRD pattern of the sample obtained after 12.5 h RBM revealed new sharp Bragg peaks related to β -MgH₂ and γ -MgH₂ overlapped with low intensity peaks corresponding to unreacted hcp-Mg (Figure 3b). The Bragg peaks related to hcp-Mg were hardly seen in the XRD of the sample obtained after 25 h, suggesting the completion of gas–solid-reaction (Figure 3c).

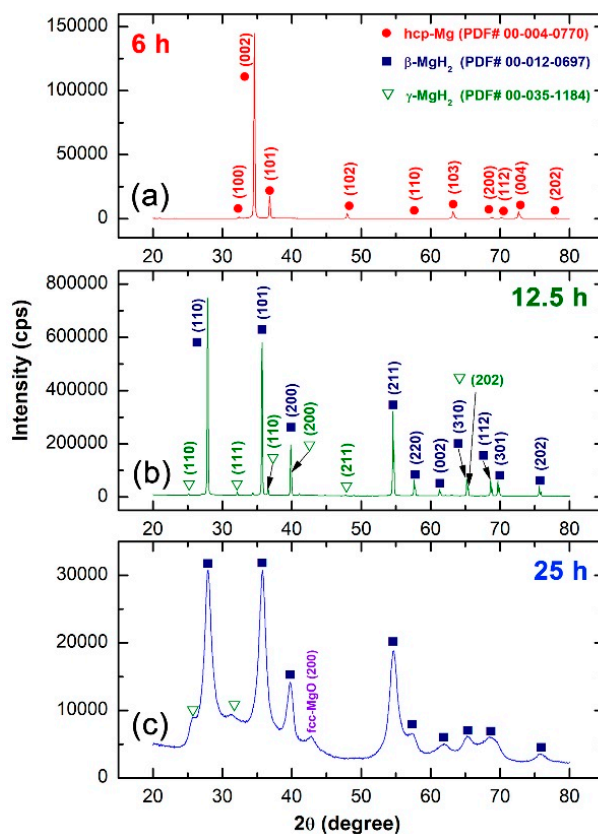


Figure 3. XRD patterns of hcp-Mg powders obtained after (a) 6 h, (b) 12.5 h and (c) 25 h of RBM time, using Zr_2Ni balls.

In contrast, when Zr_2Ni fine-shots were gradually introduced to Mg powders upon using Zr_2Ni milling media, the catalyzation process took place homogeneously, as indicated by the good distribution of Zr_2Ni grains in MgH_2 matrix (Figure 5b).

More information related to the homogeneity of MgH_2/Zr_2Ni nanocomposite powders obtained after 50 h of RBM time, using Zr_2Ni was obtained from elemental analysis performed with scanning transmission electron microscope (STEM)/X-ray elemental mapping (Figure 6). The dark gray zones shown in Figure 6a refer to corroded Zr_2Ni particles (~ 8 nm in diameter) that came from Zr_2Ni and were introduced to MgH_2 matrix (Figure 6b). These particles were embedded homogeneously in the MgH_2 matrix (Figure 6b,c) to form uniform aggregate powders 110 nm in diameter, as displayed in Figure 6a.

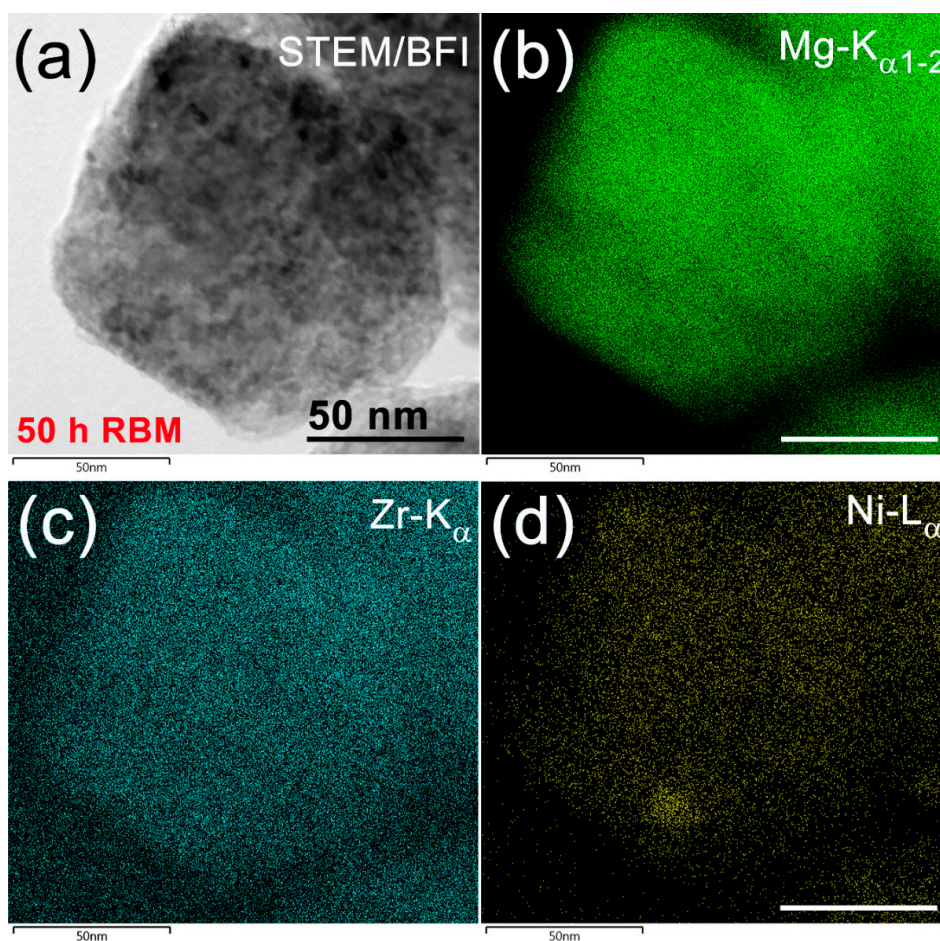
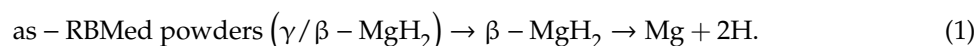


Figure 6. (a) Scanning transmission electron microscope (STEM)/BFI image of Mg powders milled under pressurized hydrogen for 50 h, using Zr_2Ni balls-milling media. The X-ray elemental mapping corresponding to $Mg-K\alpha_{1-2}$, $Zr-K\alpha$ and $Ni-L\alpha$ are displayed in (b–d), respectively.

2.4. Thermal Analysis

Differential scanning calorimetry (DSC) was conducted to study the influence of RBM time on decomposition temperature (T^{dec}) of MgH_2 doped with 5 wt% Zr_2Ni powders, using tool steel MM (Figure 7a). These results were compared with DSC results of MgH_2 powders milled for different RBM times, using Zr_2Ni balls (Figure 7b). In both figures, there are two endothermic events that refer to the decomposition of MgH_2 powders, suggesting that the decomposition process took place through two

stages of γ - β -MgH₂ phase transformation followed by decomposition of β -MgH₂ into Mg-metal and hydrogen molecule, as summarized in Equation (1);



Temperature of γ - β -phase transformation ($T_{\gamma \rightarrow \beta}^{\text{trans}}$) for MgH₂ doped with 5 wt% Zr₂Ni powders, using tool steel MM tended to decrease slightly from 678 K to 672 K after milling for 25 h and 37.5 h, respectively (Figure 7a).

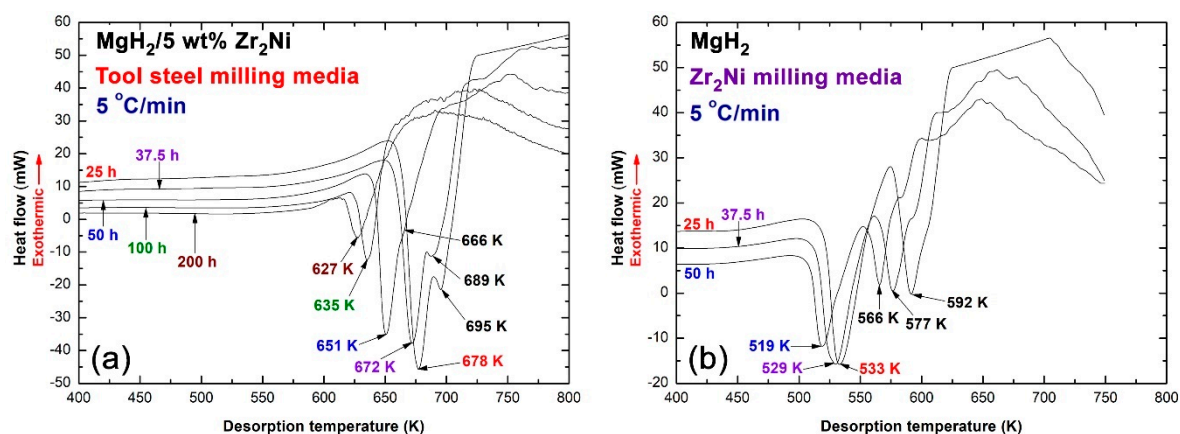


Figure 7. Normal differential scanning calorimetry (DSC) thermograms of the samples obtained after different RBM times (indexed inset of the figure) for ball milled (a) MgH₂ powders doped with 5 wt% Zr₂Ni, using tool steel balls and (b) MgH₂ powders milled with Zr₂Ni balls. All DSC measurements were conducted under 75 mL of continuous argon flow with a heating rate of 5 °C/min.

Increasing the RBM time to 50 h and 100 h led to drastic reducing on $T_{\gamma \rightarrow \beta}^{\text{trans}}$, recorded to be 651 K and 635 K respectively. This significant decrease may be attributed to the reduction of the free energy required to accomplish γ - β -MgH₂ phase transformation that was enhanced by introducing severe lattice imperfection to the powders upon further milling. It can also be attributed to the effect of the Zr₂Ni catalytic agent that became well distributed in the MgH₂ matrix. The γ -MgH₂ phase of the sample obtained after 200 h of RBM time transformed into β -phase at a lower temperature of 627 K, as shown in Figure 7a. Introducing lattice imperfection in the catalyzed MgH₂ with Zr₂Ni powders upon increasing RBM time from 25 h to 50 had obvious effect on decreasing T^{dec} of the β -MgH₂ phase, as indexed by the decomposition peak temperatures of 695 K, 678 K and 666 K, respectively (Figure 7a).

It should be noted that this two-stage decomposition is not unique for MgH₂ prepared in the present work, but it has been reported by many authors [9,11,13,36].

The $T_{\gamma \rightarrow \beta}^{\text{trans}}$ of the first endothermic peaks for MgH₂ powders milled with Zr₂Ni balls after 25 h, 37.5 h and 50 h of RBM time (Figure 7b) showed monotonical reduction with increasing RBM time from 533 K, 529 K to 519 K, respectively. Meanwhile, the corresponding T^{dec} of β -MgH₂ phase retreated from 592 K to the low temperature side of 577 K and 566 K, respectively, as shown in Figure 7b.

The apparent activation energy (E_a) of decomposition for MgH₂ powders milled with Zr₂Ni balls for 50 h was investigated by DSC with heating rates (k) of 5, 10, 20, 30 and 50 °C/min, using the Arrhenius approach in Equation (2)

$$E_a = -RT \ln(k) \quad (2)$$

where k is a temperature-dependent reaction rate constant, R is the gas constant, and T is the absolute peak temperature of decomposition. All the DSC scans revealed sharp, single endothermic events related to the decomposition of MgH₂ phase, as displayed in Figure 8a. Obviously, the peak height increased proportionally with increasing heating rates, where the peak decomposition temperatures were significantly shifted to the higher temperature side upon increasing the heating rates from

5 °C/min to 40 °C/min, as shown in Figure 8a. Taking trace of the sample conducted at 5 °C/min as a typical example, its corresponding T^{dec} was 519 K (Figure 8a). This value is far below the value (651 K) belonging to MgH₂ milled with Zr₂Ni powders for 50 h (Figure 7a). It can be concluded that milling MgH₂ with Zr₂Ni balls led to destabilizing the metal hydride phase and decreasing the decomposition temperature by 132 K. Such significant decreasing in T^{dec} is believed to be related to the homogeneous distribution of the particles from the Zr₂Ni balls and uniformly embedded into MgH₂ matrix, as shown in Figures 5b and 6.

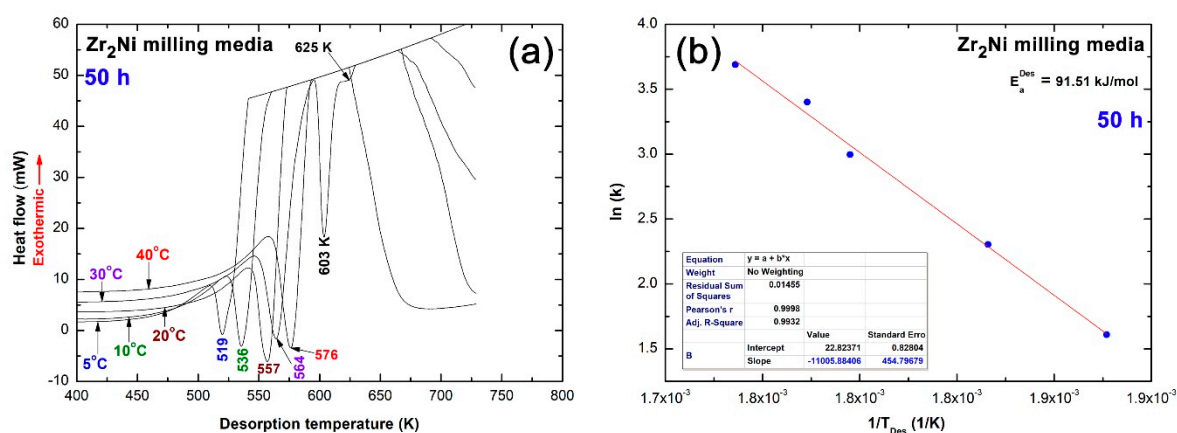


Figure 8. (a) Normal differential scanning calorimetry (DSC) thermograms of MgH₂ powders milled with Zr₂Ni balls for 50 h obtained at different heating rates (k), and (b) Arrhenius plot displaying the natural logarithmic values of k versus the inverse of the decomposition peak temperature ($1/T_{\text{Des}}$) denoted in (a).

E_a of decomposition of MgH₂ milled with Zr₂Ni balls for 50 h was determined by measuring the decomposition peak temperature corresponding to the different k and then plotting $\ln(k)$ versus $1/T_p$, as shown in Figure 8b. A best fit for the results was calculated by the least-square method. It follows from Figure 8b that all data points lie closely on the same straight line. E_a of 91.51 kJ/mol, which was obtained from the slope of the line ($-E/R$) is far below than that one obtained for pure MgH₂ nanocrystalline powders (146.53 kJ/mol [16]) and also less than the one calculated for MgH₂ milled with Zr₂Ni powders for 50 h, using tool steel balls (122.38 kJ/mol). It can be concluded here that using Zr₂Ni balls led to an outstanding improvement in the decomposition kinetics of MgH₂ powders.

2.5. De/Rehydrogenation Behaviors

2.5.1. Pressure-Composition-Temperature (PCT)

The PCT behavior of MgH₂ powders milled with Zr₂Ni balls for 50 h was volumetrically investigated by Sievert's approach at different temperatures (50 °C to 275 °C) and plotted in Figure 9a. The system revealed excellent capability for absorbing a significant amount of hydrogen (4.23 wt%) at very low temperature (50 °C), as displayed in Figure 9a. Hydrogen absorbed by Mg-active surfaces that were created by high energy milling, using Zr₂Ni balls 5 wt% was increased to higher values of 4.58 wt%, 5 wt% and 5.19 wt% upon increasing temperature to 75 °C, 100 °C and 125 °C, respectively (Figure 9a). At a rather high temperature (150 °C and 200 °C) hydrogen masses absorbed by the system were 5.32 wt% and 6.11 wt% respectively, as elucidated in Figure 9a. At this temperature, the powders corresponding to each applied temperature revealed a single reversible hydrogenation/dehydrogenation cycle (Figure 9a). Further temperature increases (225 °C, 250 °C and 275 °C) led to a slight increase in the hydrogen weight present (6.22 wt%, 6.27 wt% and 6.34 wt%, respectively). The presence of clear hydrogenation plateaus can be seen in the range between 0–5.6 wt% H₂ at the high temperature side ranging between 200 °C to 275 °C, as shown in Figure 9a. In addition, smooth desorption plateaus

were characterized in the whole hydrogen concentration range (0–5.8 wt%) for all cycles developed at different applied temperatures, as displayed in Figure 9a.

The SEM micrograph of the sample taken after the last dehydrogenation PCT cycle conducted at 275 °C is displayed in Figure 9b. The powder particles were slightly grown in size to form a large aggregate with an apparent particle size of about 100 μm in diameter (Figure 9b). This limited powder agglomeration was attributed to repetition of the hydrogenation/dehydrogenation cycles at different temperatures. The STEM/dark field (DF) image corresponding to the indexed zone shown in Figure 9b is presented in Figure 9c. After this severe domination under cyclic pressure/temperature modes, the powders still maintained their nano-dimension characterizations, indexed by the presence of nanograined Mg (light gray)/Zr₂Ni (dark gray) composite equiaxed grains with sizes ranging between 8 nm to 57 nm, as displayed in Figure 9c.

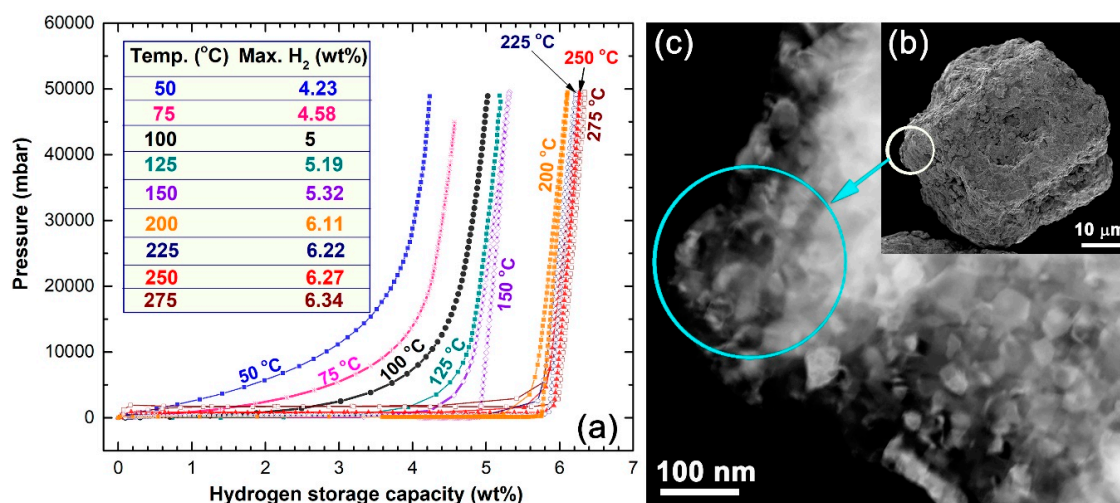


Figure 9. (a) Pressure-Composition-Temperature (PCT) curves measured at different temperatures (50 °C–275 °C) for MgH₂ powders milled with Zr₂Ni balls for 50 h, (b) SEM micrograph of the powders obeyed to PCT cycles at different temperature. The STEM/BF image of the indexed zone shown in (b) is presented in (c).

2.5.2. Hydrogenation Kinetics

Figure 10a shows the effect of RBM time on the hydrogenation kinetics for MgH₂ powders milled with Zr₂Ni balls. The measurements were conducted at 200 °C under hydrogen pressure of 10 bar. All samples obtained after different RBM times were capable of absorbing hydrogen with different scales of absorption time (Figure 10a). In general, the powder milled with Zr₂Ni balls showed better kinetics when compared with the Mg doped with 5 wt% Zr₂Ni powders milled with tool steel balls for 50 h. This is implied by the very long time required (~36085 s) to absorb 6.2 wt% H₂ at high temperature (350 °C), as displayed in Figure 10b.

The powders obtained after the early stage of RBM (12.5 h) absorbed 1.78, 3.3 and 4.53 wt% H₂ within 25, 100 and 300 s respectively, as displayed in Figure 10c. Limited improvement on the hydrogenation kinetics was obtained with increasing the RBM time to 25 h (intermediate stage), as characterized by the marginal increase in absorbed H₂ (4.88 wt%) obtained after 300 s (Figure 10c). The powders obtained after 37.5 h of RBM exhibited good absorption kinetics, as suggested by the higher hydrogen wt% (5.28) absorbed after only 300 s, as presented in Figure 10c. Towards the end of RBM processing time (50 h), where the nanocomposite powders of this final product had homogeneous composition, they absorbed higher hydrogen wt% of 4.98 and 6.1 within 100 s and 300 s, respectively (Figure 10c).

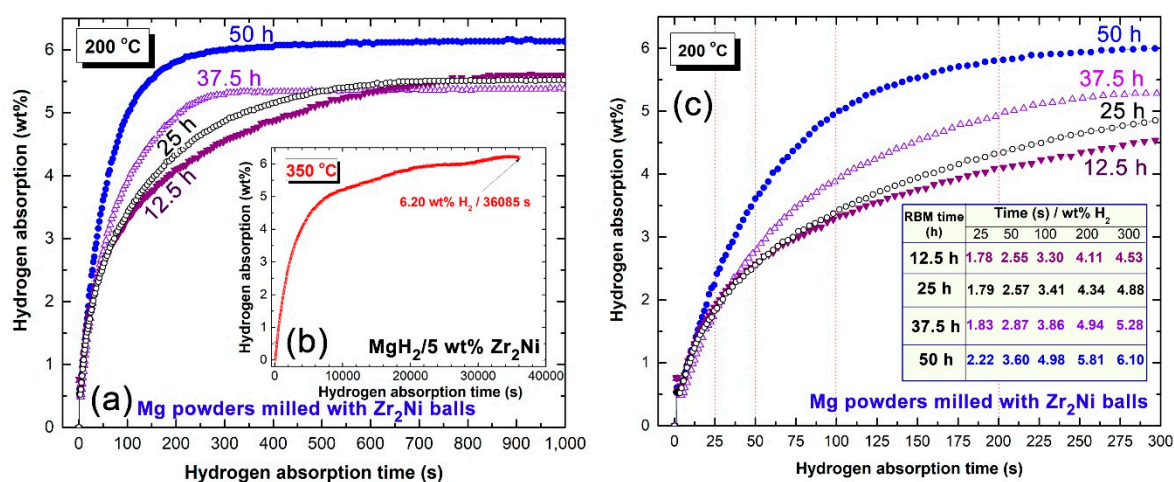


Figure 10. (a) Hydrogenation kinetics, measured at 200 °C under 10 bar of hydrogen for MgH₂ powders milled with Zr₂Ni balls after different RBM times, and (b) hydrogen absorption kinetics, measured at 350 °C under 30 bar of hydrogen of MgH₂ doped with Zr₂Ni powders and milled for 50 h. The hydrogenation behaviors of the samples shown in (a) are demonstrated in (c) with a different scale of absorption time.

Hydrogen storage capacity of the samples obtained after the early and intermediate stages of RBM (12.5 h, 25 h and 37.5 h) saturated at ~5.5 wt% after ~700 s of absorption time (Figure 10a), while the final product sample (50 h) saturated at ~6.2 wt% H₂ within 425 s, as presented in Figure 10a. When the absorption kinetics of this system are compared with the other MgH₂-based systems, it can be concluded that the present system is one of those few systems showing fast absorption kinetics at rather low temperature (200 °C) and pressure (10 bar H₂), as presented in Figure 10c.

2.5.3. Dehydrogenation Kinetics

Measuring kinetics of the hydrogen released was attained to complete the picture of MgH₂ powders milled with Zr₂Ni balls kinetics behavior for the samples obtained after different RBM times. Figure 11a demonstrates influence of RBM time on improving the dehydrogenation kinetics for MgH₂ powders milled with Zr₂Ni balls for 12.5, 25, 37.5, and 50 h. The dehydrogenation characteristics during the first few seconds of hydrogen desorption (0 s to 300 s) for these selected samples (Figure 11a) are elucidated in Figure 11b. All measurements were conducted at 225 °C under hydrogen pressure of 200 mbar.

The sample obtained after a few hours of RBM (12.5 h) showed very slow desorption kinetics, indicated by the long time required to discharge 0.2 wt% H₂, as shown in Figure 11b. These kinetics were improved by allowing longer desorption time (800 s), where the hydrogen released from the sample was close to 1.5 wt% (Figure 11a). Increasing RBM time to 25 h led to a moderate improvement, characterized by increasing the wt% of hydrogen (2.83) released after only 300 s, as displayed in Figure 11b. Further hydrogen releasing (~5.7 wt%) was attained with increasing desorption time to 800 s (Figure 11a). Outstanding improvement on the dehydrogenation kinetics was achieved for the samples obtained at the end of RBM processing time, 37.5 h and 50 h where they released 5.82 and 5.97 wt% H₂, after a very short time (300 s), as shown in Figure 11b. They reached very close values of 6.2 wt% H₂ after 700 s, where they saturated at this value even after 800 s of desorption time (Figure 11a).

The crystal structure of the 50-h sample taken after dehydrogenation and hydrogenation kinetics measurements was investigated by XRD technique. The XRD patterns of the sample taken after dehydrogenation are shown in Figure 12a,b. Obviously, the powders consisted of polycrystalline composite of hcp-Mg and tetragonal-Zr₂Ni phases, as shown in Figure 12a. Neither reacted and/or

intermediate phase(s) could be detected, as presented in Figure 12b. The hydrogenation process of this sample led to the formation of β -MgH₂ phase coexisting with Zr₂Ni, as displayed in Figure 12c.

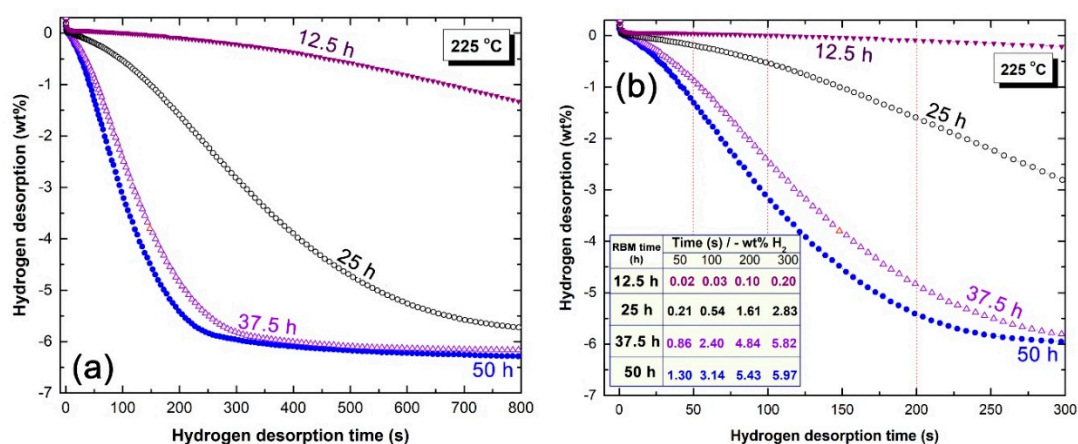


Figure 11. (a) Dehydrogenation kinetics, measured at 225 °C under 200 mbar of hydrogen for MgH₂ powders milled with Zr₂Ni balls after different RBM times of 12.5, 25, 37.5 and 50 h. The dehydrogenation behaviors of the samples shown in (a) are displayed in (b) with a different scale of desorption time.

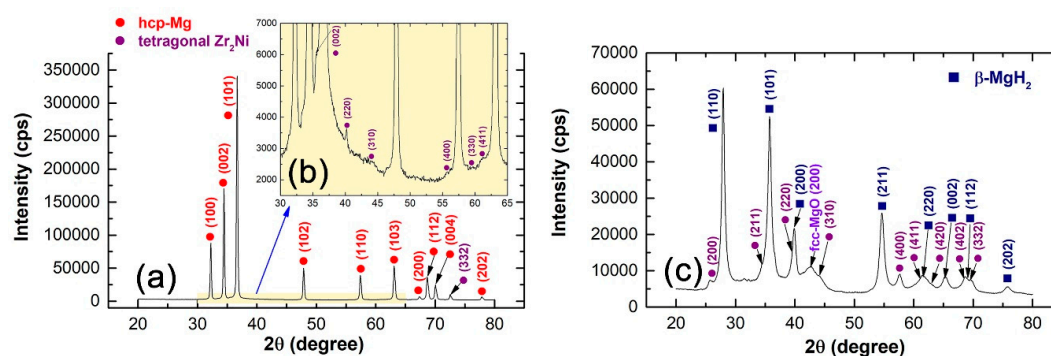


Figure 12. XRD patterns measured with CuK α radiation for 50 h-sample taken after (a,b) dehydrogenation kinetics, and (c) hydrogenation measurements.

2.5.4. Cyclability and Performance

Figure 13a displays the full profile of hydrogenation/dehydrogenation cycle-life-time test of Mg powders milled with Zr₂Ni balls under 50 bar H₂ for 50 h investigated at 225 °C, using 10 bar and 200 mbar H₂ for absorption and desorption, respectively. The sample was firstly subjected to severe heat treatment, conducted at 300 °C under 25 bar of hydrogen for 50 h. This powder activation step is necessary to breakdown the hard MgO layer coating the powder particles and to reduce the oxide phase into Mg metal and H₂O vapor, which is evacuated outside of the reactor. Accordingly, the hydrogen storage capacity of the powders increased to 6.52 wt%, as shown in Figure 13a. During the first 400 h of the test, the sample showed behavior of degradation, characterized by an obvious drop in its storage capacity that reached to ~6 wt% H₂ and kinetics decay, indicated by the rather long time (1 h) to complete 1.3 cycles, as indexed in Figure 13b.

In order to enhance the cyclability of the system and improve the powders, they were activated again for 25 h at 350 °C under 35 bar of hydrogen. Then, the cyclic test was continued at 225 °C under hydrogenation/dehydrogenation pressure of 10 and 200 mbar, respectively. In the second part of this test (400 h to 800 h), the powders revealed excellent hydrogen storage capacity (~6.5 wt%) that did not decrease upon increasing the cycle-life-time, as shown in Figure 13c. Moreover, the number of cycles achieved per one hour was significantly increased to be 1.8 cycles (Figure 13c). The hydrogen storage capacity maintained its high value of 6.5 wt% during the third stage of cycle-life-time test, extended

from 800 h to 980 h, as displayed in Figure 13d. In addition, the gas absorption/desorption kinetics was constant and did not depreciate during this stage of the test, as implied by achieving 2.3 cycles per h (Figure 13d). Figure 13e shows the last five cycles of the test, which were achieved in the range between ~ 980.5 h to 985.5 h. The results indicated that the system kept its constant value of storage capacity (~ 6.5 wt% H_2) with acceptable rate of hydrogenation/dehydrogenation that was measured to be one cycle per hour, as presented in Figure 13e.

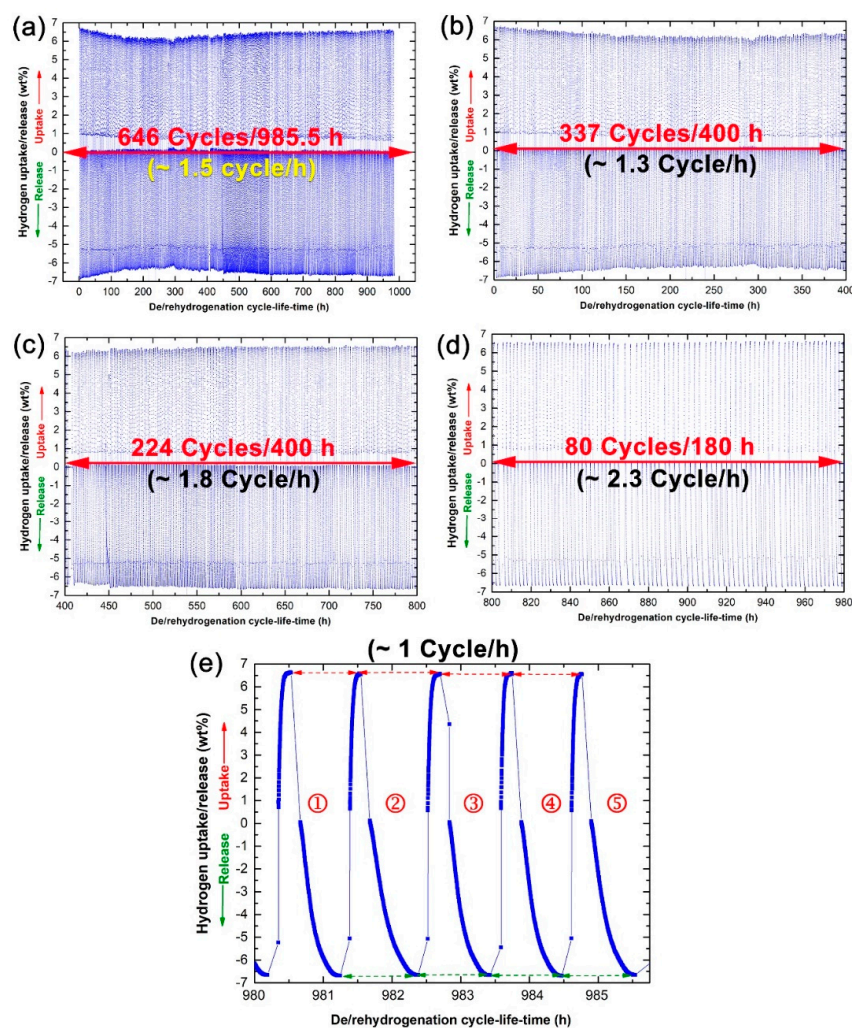


Figure 13. (a) Complete profile of cycle-life-time test conducted for 985.5 h (646 cycles) of 50-h MgH_2 powders milled with Zr_2Ni balls. The cycle-life-time curves for the first and second 400 h are presented in (b) and (c) respectively, where the last 180 h is displayed in (d). The last five cycles of the test is presented in (e). All measurements were conducted at 225 °C, with hydrogenation and dehydrogenation pressure of 10 bar and 200 mbar of hydrogen, respectively.

3. Materials and Methods

3.1. Fabrication of Zr_2Ni Ball Milling Media

Spherical Zr_2Ni balls with ~ 10 mm in diameter were prepared by the arc melting technique, using 800A-Arc Melter AM 200, provided by Edmund Bühler GmbH, Bodelshausen-Germany. In this experiment bulk Zr (99.5 wt%) and Ni (99.99 wt%) foils supplied by Sigma-Aldrich (St. Louis, Missouri, USA) were balanced to give the nominal atomic composition of tetragonal- Zr_2Ni phase. The starting foils were placed in a Cu-hearth cooled by water, where the melting process was conducted for 5 times to ensure homogeneity of the product. These spherical balls were used as milling media (MM) for

conducting reactive ball milling of Mg powders under pressure (50 bar). A part of the fabricated Zr_2Ni balls were crushed down into small pieces (~3 mm to 5 mm), using a 20-ton cold press and then ball milled under argon gas for 100 h, using a high-energy planetary ball mill operated at 250 rpm.

3.2. Preparation of MgH_2 Powders Catalyzed with Zr_2Ni Particles

Pure Mg powders (99.8 wt%, 80 μm in diameter), supplied by Sigma-Aldrich, St. Louis, Missouri, USA were used as starting materials for conducting gas–solid reactions with hydrogen gas (99.99 wt%, provided by local gas company in Kuwait). In the first experimental set, 6 g of the powders were sealed into a tool steel vial with Zr_2Ni balls of 10 mm in diameter inside a He glove box. In the second set, however, Mg powders were mixed with 5 wt% of Zr_2Ni and charged in the vial with 10 mm tool-steel balls. In both experimental sets, the ball-to-powder weight ratio was 47:1. The vials were then pressurized with H_2 gas under 60 bar before it mounted on a planetary type ball mill. The reactive ball milling (RBM) process was started for different RBM times of 6, 12.5, 25, 37.5 and 50 h. After each RBM run, the milled product was completely discharged inside the glove box, where new unprocessed powders were charged in the vial for further milling. This step was necessary to keep the ball-to-powder weight ratio constant.

3.3. Powder Characterizations

3.3.1. XRD, High Resolution Transmission Electron Microscope (HRTEM), STEM/Energy-Dispersive X-ray spectroscopy (EDS) and Inductively Coupled Plasma Mass Spectrometry (ICP-MS)

The general crystal structure of all samples was investigated by X-ray diffraction (XRD) with $Cu-K\alpha$ radiation, using 9 kW intelligent X-ray diffraction system, provided by SmartLab-Rigaku, Akishima-shi, Tokyo, Japan. The local structure of samples was studied by 2100F-field emission high resolution transmission electron microscope (FE-HRTEM) operated at 200 kV. The microscope was supplied by JEOL, Musashino, Akishima, Tokyo, Japan. Scanning transmission electron microscopy (STEM, -2100F, Tokyo, Japan), which is equipped with energy-dispersive X-ray spectroscopy (EDS) supplied by Oxford Instruments, Abingdon, UK was used to conduct elemental local analysis. In addition to EDS elemental analysis, inductively coupled plasma mass spectrometry (ICP-MS) provided by Shimadzu Scientific Instruments, Saitama, Japan was employed to get elemental analysis by a chemical analytical approach.

3.3.2. SEM

FE-scanning electron microscope (FE-SEM), provided by JEOL, Musashino, Akishima, Tokyo, Japan, operated at 15 kV was used to investigate the morphological characterizations of the powders.

3.3.3. Normal DSC

Shimadzu Thermal Analysis System/TA-60WS, Saitama, Japan, using normal differential scanning calorimeter (DSC) was employed to investigate the decomposition temperatures of MgH_2 powders with a heating rate of 5 $^{\circ}C/min$. The apparent activation energy of decomposition (E_a) for the powders obtained after different RBM time were investigated, using the Arrhenius approach with different heating rates (5, 10, 20, 30, 40 $^{\circ}C/min$).

3.3.4. De/Rehydrogenation Behaviors

The hydrogen absorption/desorption kinetics were investigated via Sievert's method, using PCTPro-2000, provided by Setaram Instrumentation, Caluire-et-Cuire, France, under hydrogen gas pressure of 200 mbar (dehydrogenation) and 10 bar (hydrogenation). The samples were examined at different temperatures of 50, 75, 100, 125, 150, 200, 225, 250 and 275 $^{\circ}C$. In this analysis, the dosed hydrogen pressure in absorption/desorption was gradually increased/decreased by 1000 mbar until equilibrium pressure reached to 13,000 and 50 mbar, respectively. The PCT absorption/desorption kinetics were fitted in real-time by the software, to determine the sufficient equilibration time (the next

point would start when the uptake had relaxed just 99% to asymptote). A minimum time of 30 min per equilibrium point and a maximum timeout of 300 min were set for each kinetic step in both the absorption and desorption isotherms.

4. Conclusions

The aim of this study was focused on preparing homogeneous MgH₂/catalytic agent (tetragonal-Zr₂Ni) nanocomposite powders with excellent hydrogen storage characteristics and cyclic performance. The work has succeeded to introduce a cost effective catalyzation process, using bulk Zr₂Ni balls as milling media. Based on the results driven from the present work it can be concluded that:

- In contrast to traditional doping and milling Mg powders with Zr₂Ni powders using tool steel balls, our proposed in-situ gradual doping Mg was successfully achieved upon using Zr₂Ni-balls milling media ball milling. This new catalyzation process has shown mutually beneficial for overcoming the agglomeration of catalytic agent in Mg matrix.
- During reactive ball milling process, corroded Zr₂Ni fine particles from Zr₂Ni balls, were introduced to Mg matrix and led to accelerate the mechanically induced gas–solid-reaction. These hard particles played a vital micro milling-media role for disintegrating Mg/MgH₂ powders to nanoscale particles after only 50 h of milling.
- Homogeneous distribution of Zr₂Ni in a MgH₂ matrix had the desired effect on decreasing the decomposition temperature of MgH₂ to 519 K with a low value of apparent activation energy of decomposition (91.51 kJ/mol).
- Drastic disintegration of MgH₂ particles conducted by Zr₂Ni particles led to a decrease in the hydrogen diffusion distance and facilitated excellent hydrogenation properties of Mg. This was realized by the powder capability to react with hydrogen at very low (50 to 125 °C) and moderate (125 to 150 °C) temperatures. The hydrogen storage capacity of the powders measured at 50 °C and 150 °C were 4.23 wt% and 5.32 wt%, respectively. At 200 °C, however, storage capacity reached to 6.11 wt%.
- MgH₂/5 wt% Zr₂Ni nanocomposite powders obtained after 50 h of milling with Zr₂Ni balls possessed superior hydrogenation kinetics at 200 °C, characterized by the short time (425 s) required to absorb 6.2 wt% H₂. This came in contrast with Mg sample doped with 5 wt% Zr₂Ni powders and milled for 50 h, using tool steel balls, which absorbed 6.2 wt% H₂ at 350 °C in 36085 s.
- Likewise the excellent characteristics of hydrogenation, the milled samples with Zr₂Ni revealed good dehydrogenation kinetics, indexed by a short time needed (700 s) to release its full storage capacity (6.2 wt% H₂).
- The powders also showed excellent cyclability for achieving a continuous 646 cycles in 985.5 h without severe degradation.
- One merit of this proposed catalyzation approach is the ability of Zr₂Ni balls to be used several times for mechanical doping of MgH₂ and maybe other metal hydride systems.

Author Contributions: M.S.E.-E. designed the experimental work, shared in sample preparation, XRD, TEM, SEM characterizations and wrote the manuscript; both F.A.-A. and M.B. equally contributed to this work by achieving the thermal analysis and kinetics measurements.

Funding: This work has been partially funded by the Kuwait Foundation for the Advancement of Sciences (KFAS) related to the Project EA078C under a contract number: PR1814SP12.

Acknowledgments: The financial support received by the Kuwait Government through the Kuwait Institute for Scientific Research for purchasing the equipment used in the present work, using the budget dedicated for the project led by the first author (P-KISR-06-04) of Establishing Nanotechnology Center in KISR is highly appreciated.

Conflicts of Interest: The authors declare no competing financial interests.

References

1. Calka, A. Formation of titanium and zirconium nitrides by mechanical alloying. *Appl. Phys. Lett.* **1991**, *7*, 1568–1570. [[CrossRef](#)]
2. El-Eskandarany, M.S.; Sumiyama, K.; Aoki, K.; Suzuki, K. Reactive ball mill for solid state synthesis of metal nitrides powder. *Mater. Sci. Forum* **1992**, *88*, 801–808. [[CrossRef](#)]
3. Montone, A.; Aurora, A.; Gattia, D.M.; Antisari, M.V. Microstructural and Kinetic Evolution of Fe Doped MgH₂ during H₂ Cycling. *Catalysts* **2012**, *2*, 400–411. [[CrossRef](#)]
4. Bhatnagar, A.; Shaz, M.A.; Srivastava, O.N. Synthesis of MgH₂ using autocatalytic effect of MgH₂. *Int. J. Hydrogen Energy* **2019**, *44*, 6738–6747. [[CrossRef](#)]
5. El-Eskandarany, M.S.; Banyan, M.; Al-Ajmi, F. Synergistic effect of new ZrNi₅/Nb₂O₅ catalytic agent on storage behavior of nanocrystalline MgH₂ powders. *Catalysts* **2019**, *9*, 306. [[CrossRef](#)]
6. Schlapbach, L.; Zuttel, A. Hydrogen-storage materials for mobile applications. *Nature* **2001**, *414*, 353–358. [[CrossRef](#)] [[PubMed](#)]
7. Jain, I.P.; Lal, C.; Jain, A. Hydrogen storage in Mg: A most promising material. *Int. J. Hydrogen Energy* **2010**, *35*, 5133–5144. [[CrossRef](#)]
8. Yartys, V.A.; Lototsky, M.V.; Akiba, E.; Albert, R.; Antonov, V.E.; Ares, J.R.; Baricco, M.; Bourgeois, N.; Buckley, C.E.; Bellosta von Colbe, J.M. Magnesium based materials for hydrogen based energy storage: Past, present and future. *Int. J. Hydrogen Energy* **2019**, *44*, 7809–7859. [[CrossRef](#)]
9. Bellosta von Colbe, J.M.; Ares, J.-R.; Barale, J.; Baricco, M.; Buckley, C.; Capurso, G.; Gallandat, N.; Grant, D.M.; Guzik, M.N.; Jacob, I. Application of hydrides in hydrogen storage and compression: Achievements, outlook and perspectives. *Int. J. Hydrogen Energy* **2019**, *44*, 7780–7808. [[CrossRef](#)]
10. El-Eskandarany, M.S.; Shaban, E.; Aldakheel, F.; Alkandary, A.; Behbehani, M.; Al-Saidi, M. Synthetic nanocomposite MgH₂/5 wt.% TiMn₂ powders for solid-hydrogen storage tank integrated with PEM fuel cell. *Sci. Rep.* **2018**, *7*, 13296. [[CrossRef](#)]
11. Rusman, N.A.A.; Dahari, M.A. Review on the current progress of metal hydrides material for solid-state hydrogen storage applications. *Int. J. Hydrogen Energy* **2016**, *411*, 12108–12126. [[CrossRef](#)]
12. Lototsky, M.V.; Tolj, I.; Pickering, L.; Sita, C.; Barbir, F.; Yartys, V. The use of metal hydrides in fuel cell applications. *Prog. Nat. Sci.-Mater.* **2017**, *27*, 3–20. [[CrossRef](#)]
13. El-Eskandarany, M.S. Recent developments on fabrication, characterization and implementation of MgH₂-based solid-hydrogen materials in Kuwait Institute for Scientific Research. *RSC Adv.* **2019**, *9*, 9907–9930. [[CrossRef](#)]
14. El-Eskandarany, M.S.; Alkandary, A.; Aldakheel, F.; Al-Saidi, M.; Al-Ajmi, F.; Banyan, M. Performance and fuel cell applications of reacted ball-milled MgH₂/5.3 wt% TiH₂ nanocomposite powders. *RSC Adv.* **2018**, *8*, 38175–38185. [[CrossRef](#)]
15. Valiev, R.Z.; Islamgaliev, R.K.; Alexandrov, I.V. Bulk nanostructured materials from severe plastic deformation. *Prog. Mater. Sci.* **2000**, *45*, 103–189. [[CrossRef](#)]
16. El-Eskandarany, M.S.; Shaban, E.; Al-Halaili, B. Nanocrystalline β-γ-β cyclic phase transformation in reacted ball milled MgH₂ powders. *Int. J. Hydrogen Energy* **2014**, *39*, 12727–12740. [[CrossRef](#)]
17. Amira, S.; Huot, J. Effect of cold rolling on hydrogen sorption properties of die-cast and as-cast magnesium alloys. *J. Alloys Compd.* **2012**, *520*, 287–294. [[CrossRef](#)]
18. El-Eskandarany, M.S.; Banyan, M.; Al-Ajmi, F. Discovering a new MgH₂ metastable phase. *RSC Adv.* **2018**, *8*, 32003–32008. [[CrossRef](#)]
19. Vajeeston, P.; Ravindran, P.; Kjekshus, A.; Fjellvåg, H. Pressure-induced structural transitions in MgH₂. *Phys. Rev. Lett.* **2002**, *89*, 175506–175509. [[CrossRef](#)]
20. Jorge, A.M.; de Lima, G.F.; Triques, M.R.M.; Botta, W.J.; Langdon, T.G. Correlation between hydrogen storage properties and textures induced in magnesium through ECAP and cold rolling. *Int. J. Hydrogen Energy* **2014**, *39*, 3810–3821. [[CrossRef](#)]
21. Moretto, P.; Zlotea, C.; Dolci, F.; Amieiro, A.; Bobet, J.L.; Borgschulte, A.; Chandra, D.; Enoki, H.; De Rango, P.; Fruchart, D.; et al. A Round Robin Test exercise on hydrogen absorption/desorption properties of a magnesium hydride based material. *Int. J. Hydrogen Energy* **2013**, *38*, 6704–6717. [[CrossRef](#)]

22. Shang, C.X.; Bououdina, M.; Song, Y.; Guo, Z.X. Mechanical alloying and electronic simulations of (MgH₂+M) systems (M = Al, Ti, Fe, Ni, Cu and Nb) for hydrogen storage. *Int. J. Hydrogen Energy* **2004**, *29*, 73–80. [[CrossRef](#)]
23. Yamada, T.; Yin, J.; Tanaka, K. Hydrogen storage properties and phase structures of Mg-rich Mg-Pd, Mg-Nd and Mg-Pd-Nd alloys. *Mater. Trans.* **2001**, *42*, 2415–2421. [[CrossRef](#)]
24. Zhou, C.; Fang, Z.; Ren, C.; Li, J.; Lu, J. Effect of Ti intermetallic catalysts on hydrogen storage properties of magnesium hydride. *J. Phys. Chem. C* **2014**, *118*, 11526–11535. [[CrossRef](#)]
25. Xiong, Y.; Ba, J.; Qing, W.; Jing, W. Hydrogen storage properties of nanocrystalline Mg₂Ni based alloys prepared by ball-milling. *J. Plasma Fusion Res. Ser.* **2013**, *10*, 94–97.
26. El-Eskandarany, M.S.; Al-Matrouk, H.; Shaban, E.; Al-Duweesh, A. Effect of mechanically-induced solid-state doping time on the morphology and hydrogenation cyclability of MgH₂/7Mn_{3.6}Ti_{2.4} nanocomposite powders. *Int. J. Hydrogen Energy* **2015**, *40*, 10139–10149. [[CrossRef](#)]
27. Ma, T.; Isobe, S.; Wang, Y.; Hashimoto, N.; Ohnuki, S. Catalytic Effect of Nb₂O₅ in MgH₂-Nb₂O₅ Ball-Milled Composites. *Catalysts* **2012**, *2*, 344–351. [[CrossRef](#)]
28. Ares-Fernández, J.-R.; Aguey-Zinsou, K.-F. Superior MgH₂ Kinetics with MgO Addition: A Tribological Effect. *Catalysts* **2012**, *2*, 330–343. [[CrossRef](#)]
29. El-Eskandarany, M.S.; Shaban, E.; Al-Shemmiri, A. Integrated Ni/Nb₂O₅ nanocatalytic agent dose for improving the hydrogenation/dehydrogenation kinetics of reacted ball milled MgH₂ powders. *Int. J. Hydrogen Energy* **2014**, *39*, 21097–21106. [[CrossRef](#)]
30. Ranjbara, A.; Guoa, Z.P.; Yua, X.B.; Wexler, D.; Calka, A.; Kimd, C.J.; Liu, H.K. Hydrogen storage properties of MgH₂-SiC composites. *Mater. Chem. Phys.* **2009**, *114*, 168–172. [[CrossRef](#)]
31. El-Eskandarany, M.S.; Shaban, E. Contamination Effects on Improving the Hydrogenation/Dehydrogenation Kinetics of Binary Magnesium Hydride/Titanium Carbide System Prepared by Reactive Ball Milling. *Materials* **2015**, *8*, 6880–6892. [[CrossRef](#)]
32. El-Eskandarany, M.S. Metallic glassy Zr₇₀Ni₂₀Pd₁₀ powders for improving the hydrogenation/dehydrogenation behavior of MgH₂. *Sci. Rep.* **2016**, *6*, 26936. [[CrossRef](#)]
33. El-Eskandarany, M.S. Metallic glassy Ti₂Ni grain-growth inhibitor powder for enhancing the hydrogenation / dehydrogenation kinetics of MgH₂. *RSC Adv.* **2019**, *9*, 1036. [[CrossRef](#)]
34. El-Eskandarany, M.S.; Saeed, M.; Al-Nasrallah, E.; Al-Ajmi, F.; Banyan, M. Effect of LaNi₃ Amorphous Alloy Nanopowders on the Performance and Hydrogen Storage Properties of MgH₂. *Energies* **2019**, *12*, 1005. [[CrossRef](#)]
35. Ismail, M. Effect of LaCl₃ addition on the hydrogen storage properties of MgH₂. *Energy* **2015**, *79*, 177–182. [[CrossRef](#)]
36. Sun, Y.; Shen, C.; Lai, Q.; Liu, W.; Wang, D.-W.; Francois, K.; Zinsou, A. Tailoring magnesium based materials for hydrogen storage through synthesis: Current state of the art. *Energy Storage Mater.* **2018**, *10*, 168–198. [[CrossRef](#)]
37. Xia, G.; Tan, Y.; Chen, X.; Sun, D.; Guo, Z.; Liu, H.; Ouyang, L.; Zhu, M.; Yu, X. Monodisperse Magnesium Hydride Nanoparticles Uniformly Self-Assembled on Graphene. *Adv. Mater.* **2015**, *27*, 5981–5988. [[CrossRef](#)] [[PubMed](#)]
38. Xia, G.; Tan, Y.; Wu, F.; Fang, F.; Sun, D.; Guo, Z.; Huang, Z.; Yu, X. Graphene-wrapped reversible reaction for advanced hydrogen storage. *Nano Energy* **2016**, *26*, 488–495. [[CrossRef](#)]
39. Zhang, H.; Xia, G.; Zhang, J.; Sun, D.; Zaiping, G.; Yu, X. Graphene-Tailored Thermodynamics and Kinetics to Fabricate Metal Borohydride Nanoparticles with High Purity and Enhanced Reversibility. *Adv. Energy Mater.* **2018**, *8*, 1702975. [[CrossRef](#)]
40. El-Eskandarany, M.S.; Shaban, E.; Ali, N.; Aldakheel, F.; Alkandary, A. In-situ catalyzation approach for enhancing the hydrogenation/dehydrogenation kinetics of MgH₂ powders with Ni particles. *Sci. Rep.* **2016**, *6*, 37335. [[CrossRef](#)]
41. El-Eskandarany, M.S.; Shaban, E.; Ali, N.; Aldakheel, F.; Alkandary, A. Method of Synthesizing MgH₂/Ni Nanocomposites. US Patent 9,828,245 B1, 28 November 2017.

